Temporal and spectral dispersion of an optical source using a micromirror array-based streak camera

David M. Benton *
Aston University, Aston Institute of Photonic Technologies, Birmingham, United Kingdom

Abstract. The digital micromirror device (DMD) is an array of tilting micromirrors, capable of high frame rates that are made possible by rapid changes of angular state. The rapid angular change of the mirrors is used to sweep an optical signal across a camera sensor, resulting in a version of a streak camera, capable of temporal dispersion of an optical signal. Using a single pixel or single line of pixels can produce a continuous temporal track, whereas a two-dimensional array of mirrors scans an intensity envelope across discrete diffraction orders. Temporal resolutions of 10nS have been achieved and used to measure laser pulse widths. Combining with a diffraction grating oriented orthogonally to the temporal dispersion enables temporal and spectral dispersion to be obtained simultaneously. [DOI: 10.1117/1.OE.61.11.114108]

Keywords: micromirror array; streak camera; diffraction.

Paper 20221094G received Sep. 22, 2022; accepted for publication Oct. 31, 2022; published online Nov. 18, 2022.

1 Introduction

The digital micromirror device (DMD) is an array of rapidly tilting micromirrors that has found a primary role within digital projection technology.[1] A typical device consists of an array of around 1 million addressable mirrors each with a size of the order of 10 μm, which tilt at ± 12 deg thus providing a binary method of spatial light modulation. The micromirrors can be flipped between states at rates of 10s of kHz and this modulation speed is a significant advantage over alternative spatial light modulators (SLM) such as liquid-crystal based devices, which will achieve a few hundred Hz. This rapid binary modulation is used to provide controlled intensity levels through a pulse width modulation approach. The versatility of the DMD, its rapid modulation rate, insensitivity to polarization, relatively low cost, and robust nature have led to a diverse range of uses.[2] Applications include spectroscopy,[3] switching,[4] single pixel remote sensing,[5] laser glare suppression,[6] beam steering,[7] wavelength measurement,[8] and coherence measurement[9] to name a selection. The DMD has also found applications in biophotonics[10] and healthcare.[11] A popular area of application within physical sciences is that of wavefront control with the DMD able to produce mode structures leading to Laguerre–Gaussian and Hermite–Gaussian beams,[12] Orbital angular momentum vortex beams,[13] and wavefront control using Zernike modes for atmospheric wavefront generation[14] or improving beam quality.[15] Several review articles describe the function of the DMD and how to describe its optical field using diffraction theory.[16–18]

The speed and spatial addressing of the DMD device are properties that clearly benefit its use as an SLM, but one characteristic property that has seen very little utilization is that of the rapid angular sweep that accompanies the micromirrors changing state. Each mirror is like a small galvanometer mirror rapidly sweeping between -12 deg and $+12$ deg ("off" and "on" positions) with the potential to sweep a reflected beam through 48 deg in a short time. The speed of angular sweep arises from the small size and low mass of the individual mirrors. Alternative approaches such as rapidly spinning mirrors require robust engineering to contain the rotational energy, have longer start-up and shut-down times and require more power than a DMD. This rapid angular sweep has been used as part of an angular spatial light modulator[19] and as a

*Address all correspondence to David M. Benton, d.benton@aston.ac.uk

scanning component in a LIDAR system.[20,21] In each case, a laser pulse was synchronized with the mirror transition and delayed so as to reflect at specific angles. The laser pulse is much shorter than the transition period, effectively freezing the mirror in position. In the work reported here, the intention is to use the angular sweep as a method of temporal dispersion – rather than to use the temporal dispersion as a method of angular sweep as in the lidar systems. If light reflected from the DMD midtransition is swept across a sensor array such as a CCD then, in its simplest form, the "track" that is recorded will represent the temporal evolution of the light source during that sweep. In this form the DMD and CCD have formed a version of a streak camera.[22–24] The incoming light can be predispersed with a grating before the DMD in a direction orthogonal to the sweep direction, such that the "image" recorded by the CCD is an instantaneous two-dimensional (2D) map of the temporal and spectral characteristics of the light source.

The diffraction pattern resulting from interaction with the DMD is a messy and complicated one. Diffraction into a number of orders is responsible for the relatively poor efficiency of the device, which is dependent upon the angle of incidence but can typically be <10%. In this work, a different approach is presented on how to represent the DMD as a 2D grating and how to model expectations of a dynamic grating.

The collective diffraction behavior of the mirrors results in specific orders being present and as the mirror sweeps the reflected intensity transitions between orders, rather than a desirable continuous transition. The work that follows shows how to achieve a continuous temporal transition for use with pulse width measurement of a laser source. A demonstration of temporal and spectral dispersion is shown using an LED.

2 DMD as a Two-Dimensional Diffraction Grating

Here use is made of the approach given by Harvey and Pfisterer[25] where the incoming beam is considered relative to the geometry of the grating. The incoming beam is quantified in terms of the direction cosines in the plane of the grating. This is the point at which the incoming beam strikes the unit circle and is projected down onto the plane of the grating. The direction cosines taken in two orthogonal directions in the plane of the grating are given by two coordinates (a, b). It is easiest to consider a conventional grating aligned with the b axis but this is in fact completely arbitrary. The beam reflected and exiting close to specular reflection is considered the zeroth order and exits with the same amplitude of b as the input. Diffracted orders are separated by an angle $m\lambda/d$ where m is the diffraction order, λ is the wavelength and d is the grating feature spacing. This is shown in Fig. 1. Thus orders are represented in direction cosine space as

$$\alpha_m = \alpha_i + m\frac{\lambda}{d}, \tag{1}$$

$$\beta_m = -\beta_i, \tag{2}$$

where m is the order number and

$$\alpha_m = \sin\,\theta_m \cos\,\Phi_0, \tag{3}$$

$$\alpha_i = -\sin\,\theta_0 \cos\,\Phi_0, \tag{4}$$

$$\beta_i = -\sin\,\Phi_0, \tag{5}$$

where θ and Φ are the orthogonal angles with θ_0 being the direction of the zero order in the α direction and Φ_0 the angle in the b direction. The subscript i refers to the input beam direction. The distributions of direction cosines of diffraction orders in the grating plane are shown schematically in Figs. 1(b) and 1(c), which show the positions of diffraction orders when the grating orientation differs by 90 deg. It is important to clarify that these represent the possible beam direction for diffraction but do not reflect the amplitude of orders, which will be geometry dependent. A 2D grating such as a DMD will produce a 2D set of diffraction orders as shown in diagram c. Orders that fall outside of the unit circle are evanescent. This map of order positions is

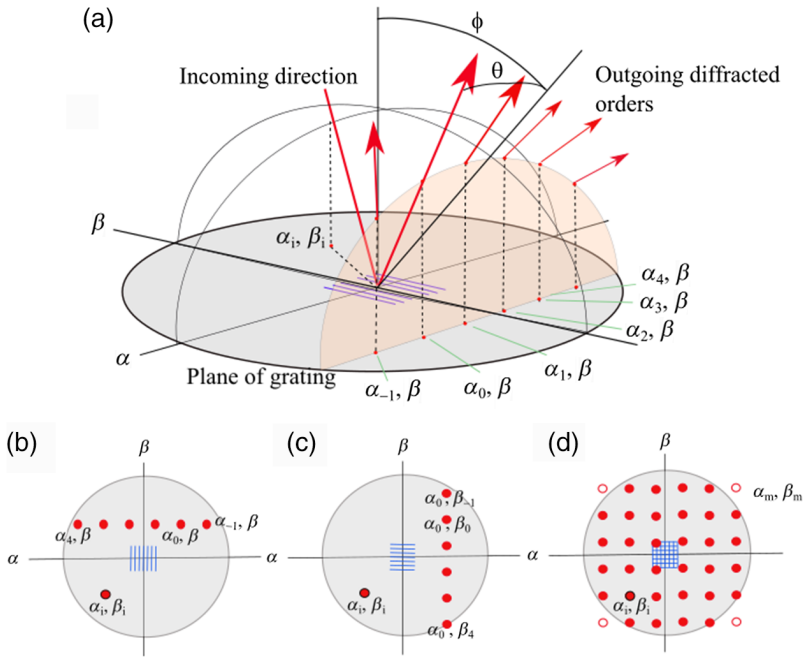

Fig. 1 (a) A schematic diagram representing how the direction cosines of incoming and diffracted beams are represented. Direction cosines of incoming and diffracted beams for (b) vertical and (c) horizontal orientations of grating. A representation of diffraction orders in a 2D grating is shown in (d).

linear due to projection onto the unit sphere and in the real world, where such orders may be viewed on a flat screen, the order spacing will become nonlinear. However, the linear spacing provides us with a usable way of modeling effects on a DMD. We can produce a grid in cosine direction space representing the orders and modulate the intensities at each order to represent particular diffraction characteristics, such as are influenced by the mirror angles, which look like a blazed grating.

The angular spacing between orders is

$$\Delta\theta = \lambda/d \tag{6}$$

and thus the number of orders in one direction is given as

$$\text{floor}(1/\Delta\theta). \tag{7}$$

The orders can be represented by a 2D comb function

$$\text{orders} = \delta(m\Delta\theta, n\Delta\theta) \tag{8}$$

And are bounded within a circle such that

$$\text{orders} = 1 \quad \text{if } (m\Delta\theta)^2 + (n\Delta\theta)^2 \leq 1 \quad = 0 \text{ otherwise.} \tag{9}$$

The DMD mirrors are at a blaze angle of -12 deg when "off" and $+12$ deg when "on." Thus the closest order number to the reflected (local zero) order is given as

$$\text{nint}\left(2 * \frac{\theta_b}{\Delta\theta}\right), \tag{10}$$

where θ_b is the blaze angle and nint() is the nearest integer. The envelope of intensity distributions is determined by the mirror size (w) and the mirror spacing (e)[17]

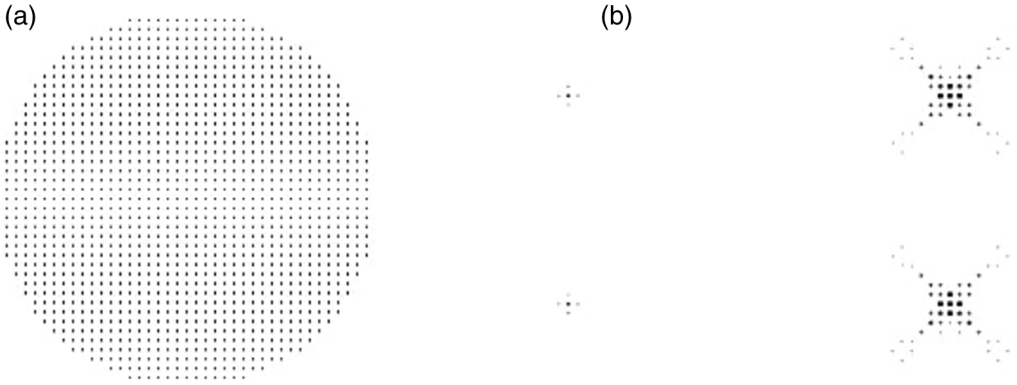

Fig. 2 (a) The full order space for a DMD and a wavelength of 635 nm. Color scale is inverted for clarity. The center plot shows the "off" and "on" diffraction positions. (b) A saturated version of the center representing a view more commonly seen when observing by eye.

$$I(\theta) = \text{sinc}\left(\frac{\theta - \theta_b}{\Delta\theta}\frac{w}{w+e}\right)^2, \tag{11}$$

and is centered on the blaze order.

Thus the intensity distribution is given as

$$I(\theta) * \text{orders}, \tag{12}$$

in direction cosine space. In the real world, each order has a physical beam size that is related to the input beam size incident on DMD (ignoring diffraction effects from any pattern present on the DMD).

Figure 2 shows how the cosine space is populated with allowed orders and how the blazed nature of the mirrors in "off" and "on" positions selects a subset of these orders. This shows intensity distributions for mirrors of 10.8 μm and a wavelength of 630 nm. The mirror spacing is not known (commercially sensitive) and is chosen here to be 1 μm, with results being indicative only. The full scale represents the full direction cosine space, which covers some ± 19 orders. The mirror tilt direction is vertical in these plots with the mirror x and y axes at 45 deg. This can be seen in the final plot, which is overexposed, showing many of the weaker orders at 45 deg to the tilt direction and represents a more complex view most often seen by users reflecting lasers from a DMD.

As the mirrors transition between the "off" and "on" states, the envelope function transitions between the two states, populating the orders between them. The blaze order then becomes time dependent

$$I(\theta) = \text{sinc}\left(\frac{\theta - \theta_b\,(t)}{\Delta\theta}\frac{w}{w+e}\right)^2, \tag{13}$$

as represented in Fig. 3 where two close times are displayed overlapping near the center of the plot, with the "off" and "on" positions also shown. This one-dimensional (1D) plot is made along the tilt axis plane. If the transition time is known, then the order intensity distribution can be used to determine the relative time from the transition start (in whichever direction). To observe orders at an intermediate position would require a pulsed laser to freeze the action. The relative delay of the laser pulse determines the position, the length of the laser pulse causes broadening of the individual orders and is a convolution of the pulse width and the order size, where the pulse width time is translated into an angular spread with a timescale related to the ratio of the pulse width to the transition time.

From this, we can see that the sweeping action of the rotating mirror sweeps the diffraction envelope function across the permissible orders thus inferring temporal pulse properties such as pulse width will require a measurement of the envelope function and an accurate understanding of the intrinsic envelope function, which is being convolved with a pulse.

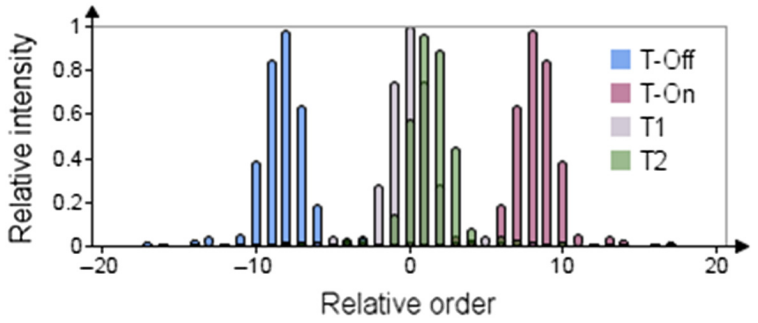

Fig. 3 DMD order distributions as the mirrors transition between initial state T0 to final state T' via intermediate states T1 and T2.

This approach represents a straightforward way of understanding the diffraction effects from a 2D dynamic blazed grating. The DMD is however not a true blazed grating as it directs light into multiple orders, it is only similar to a blazed grating. However, as we shall see in the following sections, simpler diffraction results can be obtained when using just a single mirror or a 1D line of transitioning mirrors.

3 Method and Results

The temporal dispersion that can be observed with a DMD and a camera has the system behaving like a streak camera, which will be referred to as a micromirror array-based streak camera. However, as was shown in the previous section the temporal information resides in the characteristics of the envelope (i.e., central position and width) across discrete diffraction orders. A continuous temporal dispersion can be obtained by flipping just a single mirror as no collective diffraction is involved. A third option is to flip a single line of mirrors oriented orthogonally to the tilt direction. In this case, the temporal dispersion remains continuous and collective diffraction occurs orthogonally in this direction. All three approaches will be presented in the following sections, along with a wavelength dispersion to allow both temporal and chromatic characterization of a source.

The DMD system used in this work was a DLP 7001 system from Vialux GmbH, with an array size of 1024×768 pixels. The USB control for this system allows the writing of frames as 1-bit images or multibit images with an equivalent pulse width modulation function used to control the amplitude. The device head was mounted in a 3D printed support with the DMD rotated at 45 deg, allowing the diagonal mirror pivots to be parallel to the optical table for easier alignment.

The system produced an output trigger pulse when the mirrors begin to transition. The main laser used was a variable pulse width laser (NPL64C, Thorlabs) capable of selecting pulse widths between 5 and 129 ns with a wavelength of 640 nm at a triggerable rate up to 50 kHz. Other lasers such as a HeNe were used where needed. A Stanford instruments DG535 was used to provide precise delay and pulse control for triggering the laser.

A monochrome USB camera DCC3240X (1.3 Mpixel, 10 bit) was used to capture images. Control of the DMD and image capture from the camera was performed using bespoke LabView programs. The computer would write binary frames for the choice of mirrors to use and the "picture time" for which the mirrors are held in the "on" position. The computer would also control the image captured by the camera and the exposure time. The delay used to trigger the laser, and the pulse width produced by the laser was controlled manually. This is shown schematically in Fig. 4.

3.1 *Single Mirror Temporal Dispersion*

A microscope objective was used to focus the laser light into a small spot and a single mirror flipped, with the reflected beam observed on a screen and the camera capturing the screen image.

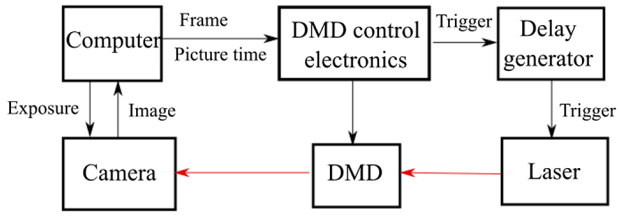

Fig. 4 A schematic diagram of the control structure. Red lines indicate light transfer.

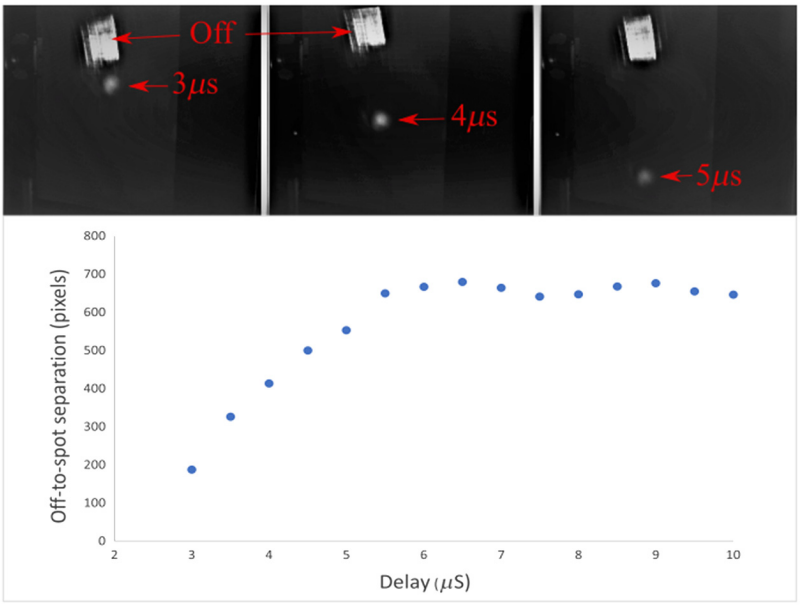

Fig. 5 Reflected beams from a single flipping mirror with various delays. The lower plot shots distance from "off" position to delayed spot with respect to delay time.

The large divergence from the DMD, coupled with the close proximity of the microscope objective made direct capture onto the camera sensor impossible. A single reflected beam spot could be observed on a screen, whose position varied with the chosen delay, as can be seen in Fig. 5. The "off" position is always seen because the mirrors always return to the "off" position before each frame and the camera is integrating. By measuring the distance between the delayed beam and an "off" feature, an estimate for the transition time of the mirror could be obtained. The plot in Fig. 5 shows the displacement as a function of delay time. The mirror completes its transition from "off" to "on" positions after 6 μs, but then shows evidence of a slight bounce before settling at around 10 μs. There is a 2 μs delay before the mirror begins to move (relative to the output trigger).

3.2 *Single Line of Mirrors*

A lens was used to focus the pulsed laser coincident with a line of mirrors orthogonal to the tilt direction. The reflected beams were intercepted by a diffusing glass plate close to the DMD (2 cm away) such that the "off" and "on" beams were both incident upon the plate. Light scattered from the plate was imaged to a camera sensor as shown schematically in Fig. 6. Images of the reflected beam for differing delay times, in steps of 100 ns, are shown in Fig. 7. The images show a diffraction pattern predominantly in the horizontal direction, the direction of the line of mirrors. Note because the focal spot size is greater than a single mirror, there is residual structure from diffraction of the neighboring "off" state mirrors. Also the diffuser scatters light predominantly in the forward direction and gives strongest signals in the center, around the 4 μs point.

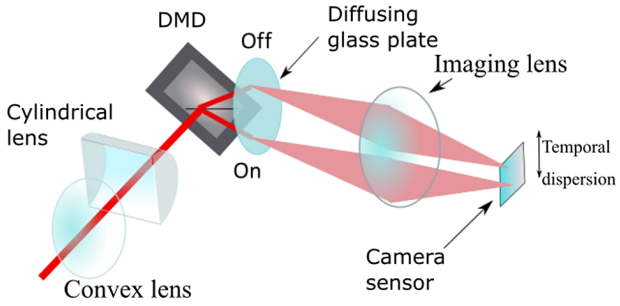

Fig. 6 A diagram of the system to capture reflected light from a single line of mirrors using a diffusing plate.

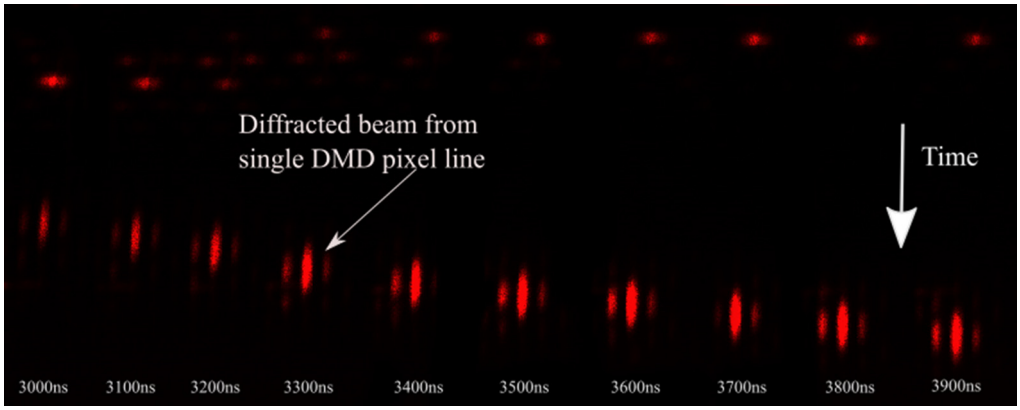

Fig. 7 A compilation of images of a reflected beam imaged from a diffusing plate, showing the relative position as the laser is delayed relative to the mirror transition.

This allows the time direction to be calibrated at 10 ns/pixel. The temporal resolution is proportional to the DMD to diffuser screen distance hence resolutions of around 1 ns/pixel could be achieved by increasing this distance to around 20 cm. With the delay fixed to place the beam centrally, images were captured of the reflected beam with differing pulse widths. From these images the vertical intensity was projected as can be seen in Fig. 8. As the pulse width is reduced so is the pulse energy hence a reduction in intensity. A Gaussian function was fit to the projected intensity to extract the center position and width. Projected pulse width vs laser pulse width is shown in the lower plot of Fig. 8. At the smallest widths, the image is dominated by intrinsic width of the reflected beam, with the pulse width effect being subpixel.

3.3 *Multiple Lines of Mirrors*

Switching multiple lines of mirrors at once will result in a 2D diffraction pattern as shown earlier but will have the advantage of higher intensity signals as more of the incident power is reflected in the sweep. In this case we are interested in relating the centroid of the whole received diffraction pattern to the temporal position. As for the single line case the vertical intensity is projected and the centroid is calculated for a known delay applied to the laser pulse. Figure 9(a) shows a captured diffraction pattern and Fig. 9(b) shows a set of projected vertical intensities showing how the pattern evolves for delay increments of 10 ns. Figure 9(c) shows a plot of centroid position versus delay which is approximately linear. However, the images of diffraction patterns do not show a smooth evolution, as might be inferred from the asymmetric intensity distribution in (a), suggesting that the actual diffraction is more complicated than presented earlier. This makes it more difficult to achieve accuracy and resolution with multiple lines than for a single line.

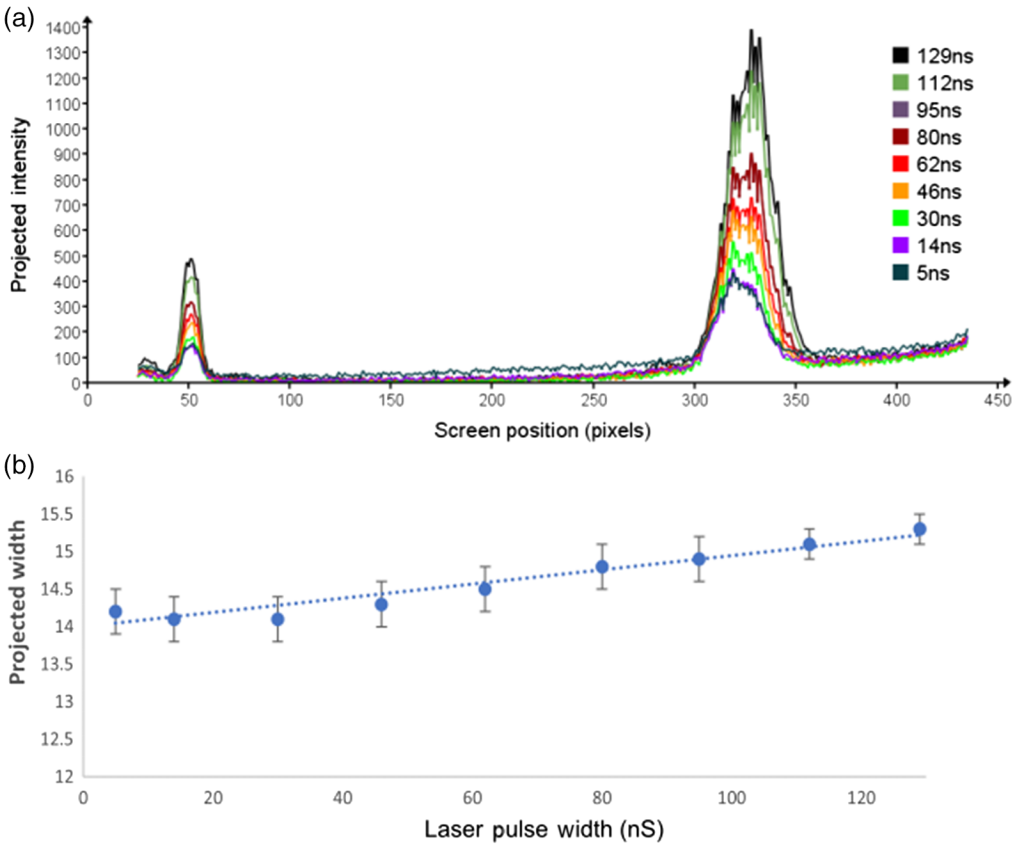

Fig. 8 (a) Vertical projections of intensity distribution for images with differing pulse widths. (b) Lower plot shows projected image width versus laser pulse width.

3.4 *Chromatic and Temporal Discrimination*

Predispersing the light with a grating before it interacts with the DMD allows both chromatic and temporal characteristics to be observed. A blazed diffraction grating (300 lines/mm) dispersed light from a fiber collimator in a direction orthogonal to the temporal dispersion. This dispersion produced a lateral wavelength displacement on the diffusing glass plate, which was imaged onto a camera—as shown in Fig. 10. To demonstrate the chromatic dispersion, three different lasers were combined using beam splitters and focused into a single mode fiber. The wavelengths red (632 nm), green (532 nm), and blue (405 nm) were used to show the extent of the chromatic dispersion but as the lasers are all continuous there is no temporal dispersion to be shown (or rather the continuous temporal nature is displayed). The grating was chosen to show the range of wavelengths together on the diffusing glass, but a more finely ruled grating with greater dispersion would have better spectral resolution if required. A photo of the diffusing glass plate is shown in Fig. 11. This photo was taken with a phone camera but the normal camera used was a monochrome USB camera where exposure time and gain can be controlled. From the photo, it can be seen that orders follow a curved path, which can be described with a quadratic function. A quadratic fit of peak-order intensity against wavelength was used to calibrate the chromatic scale. The order spacing is seen to reduce as expected for shorter wavelengths. This chromatic dispersion is then used to calibrate the horizontal wavelength scale.

Adequately demonstrating the temporal and spectral dispersion at the same time cannot be done with a single pulsed laser, and a white LED was therefore used. The LED was connected directly to the DG535 pulse generator, producing 1 μS long pulses with a controllable delay relative to the mirror flip. For consistency, the light was delivered to the DMD from the fiber collimator and this required the use of a multimode (50 μm core) fiber butted against the LED to collect as much light as possible. The signal levels were very low and required a long frame

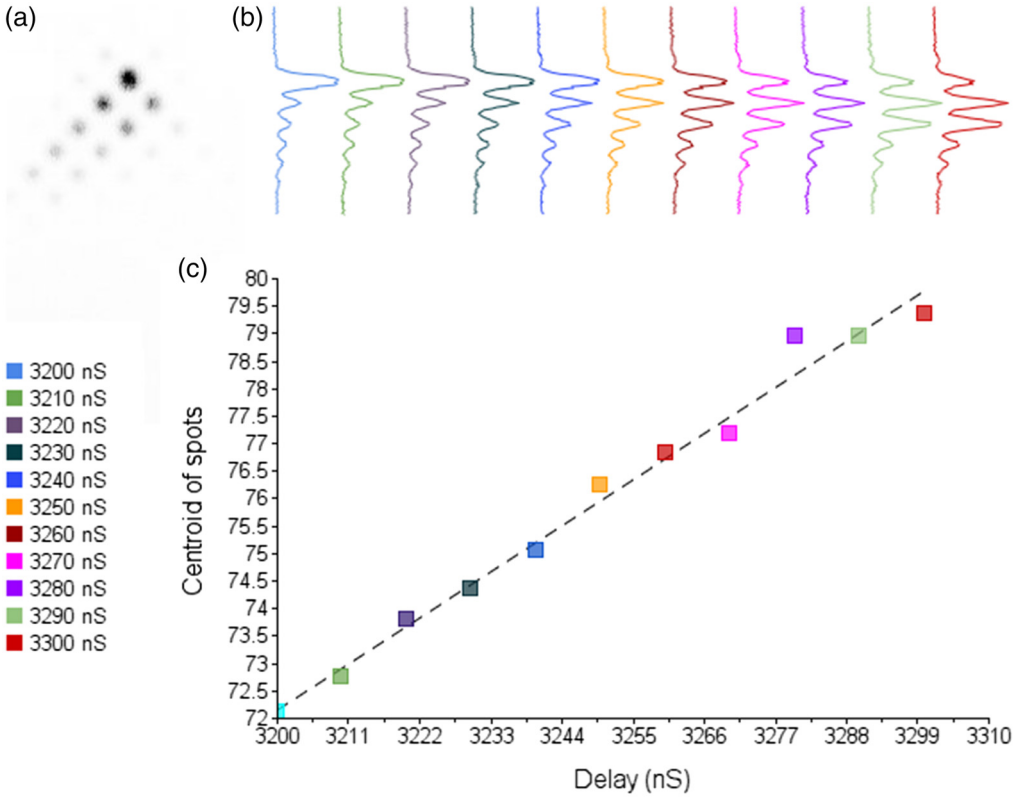

Fig. 9 (a) Diffraction pattern from a 2D array of mirrors with a laser delay of 3280 ns, (b) projected profiles for various delays, and (c) a plot of delay vs. centroid position.

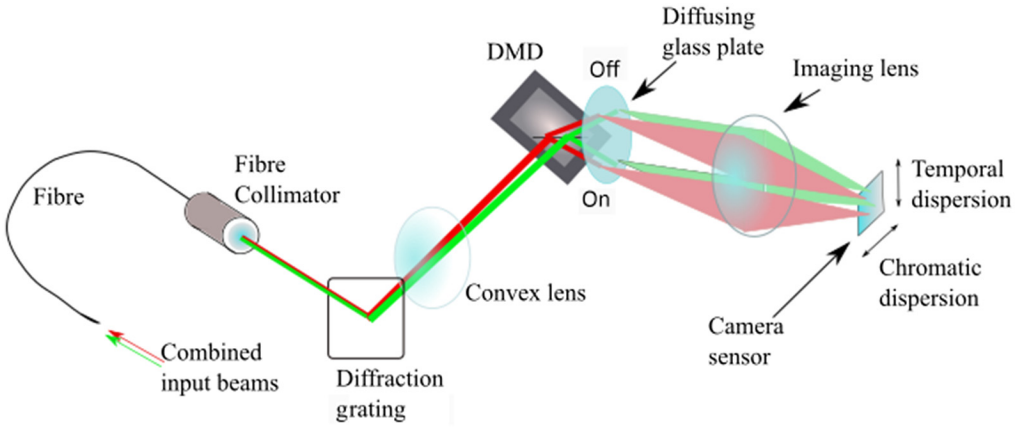

Fig. 10 A diagram of the setup for temporal and chromatic dispersion.

integration time of 137 ms (corresponding to around 900 LED pulses) and the switching of multiple pixel lines on the DMD. The use of a multimode fiber produces larger image spots and reduces resolution but was necessary to deliver sufficient light. An image of the captured pulse is shown in Fig. 12 (shown with intensity inverted for clarity) with a projection in wavelength shown below the image and a projection in the time direction to the side. The wavelength projection was taken in a region through the center of the image, with the wavelength calibration made using the same region using known wavelength lasers similar to Fig. 11, but using the monochrome camera. The temporal scale was established using images captured with different delays (3.3, 3.7, and 4.0 μS) with the image shown being delayed by 3.7 μS. The projection

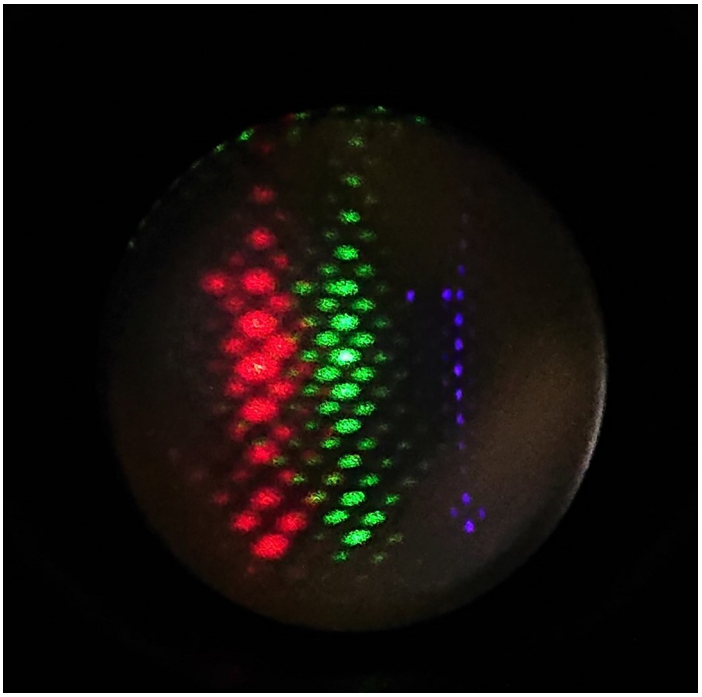

Fig. 11 Chromatic dispersion of red, green, and blue continuous lasers from a phone photo of the diffusing glass plate.

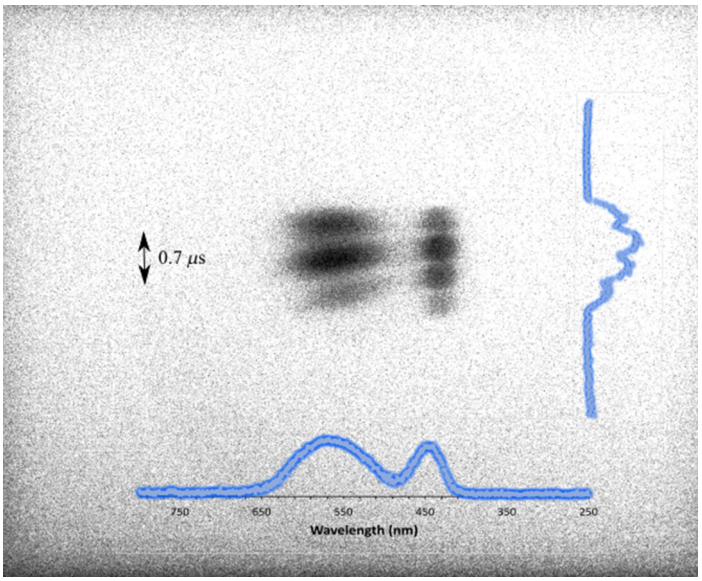

Fig. 12 An image (inverted intensity) of a pulsed white LED showing spectral and temporal dispersion.

shown is for the right-hand cluster of features and the centroid for each image was found from within this region, allowing the temporal scale to be determined as marked on the figure. This is intended only to demonstrate the principle of simultaneous wavelength and time dispersion and the production of a wavelength-time map. The spectral distribution shows good agreement with the expected spectrum for a cool white LED, with a blue LED source around 450 nm and a yellow phosphor at a longer wavelength.

4 Conclusion

The rapid change of tilt state of an array of micromirrors has been the key factor in the success of the DMD enabling its ability to rapidly rewrite spatial patterns. However, the accompanying sweep of a reflected beam as the mirrors transition between states has not been used. This work has shown that capturing a swept beam with a camera sensor array allows the temporal properties of an optical source to be captured. The combination of DMD micromirror array and camera sensor detector array forms a version of a streak camera but made from commercially available, relatively low-cost components. The micromirror array behaves in a fashion similar to a dynamic blazed diffraction grating where the blaze angle varies with time as the mirror flips. A swept reflected beam has been observed from a single micromirror—avoiding diffraction structure, a single line of mirrors—with diffraction structure in a direction orthogonal to the sweep, and a 2D array of mirrors and where the reflected optical power envelope moves across diffraction orders. Using a single line of mirrors, the observed temporal "streak" length correlates with the controlled pulse width from a laser. In the setup chosen, the pulse width was measurable down to 20 nS where the width became subpixel for the camera. Using a 2D array of mirrors, envelope shifts corresponding to 10 nS of temporal shift were observed. By predispersing, the incident light the streak camera could observe both wavelength and temporal characteristics. While a pulsed laser is ideal for demonstrating the temporal dispersion ability of the streak camera, a multiwavelength pulsed source is required to demonstrate the combined wavelength and temporal dispersion. A white light LED was used for this purpose, where a 1 μs pulse was coupled into a multimode fiber and dispersed. The weak signal levels required integration and the use of multimode fiber affected the potential resolution but nevertheless demonstrated that a DMD-based streak camera can achieve spectral and temporal dispersion.

The temporal resolution was defined by the distance of the diffuse glass screen from the DMD and was chosen to encompass the majority of the "off" to "on" transition of the mirror flip within the field of view of the camera. Moving the screen and camera further from the DMD will reduce the captured temporal dynamic range but will improve temporal resolution, which could achieve sub ns resolution. The spectral resolution was determined by the predispersion grating, which again was chosen for a wide capture range (red to blue) to demonstrate the concept. The use of a finer grating will improve spectral resolution at the expense of instantaneous spectral range—as is the case in most grating-based spectrometers. As was the case for the temporal resolution, increasing the DMD to diffuser screen distance will also linearly increase the spectral resolution (with focus adjustment to focus on the screen) thus translating the screen and camera in unison can be used to zoom the temporal and spectral resolutions. In the current setup the forward scatter function of the diffusing glass screen affects the apparent brightness, reducing intensity away from the center. This however is quite beneficial as it suppresses the endpoints as they are very much brighter than the transition.

One limitation that occurs when using a 2D array of mirrors is the depth of knowledge of the diffraction pattern that ensues. The relatively simple model of a 2D diffraction grating presented here is useful in understanding the DMD diffraction behavior but there are clearly deviations from this in the observed data. For example, the image of the captured orders using multiple lines shows clear asymmetry and structure, which can be observed in the centroid position with time Fig. 9.

The micromirror array-based streak camera can find application for characterizing an optical source, such as received unknown laser source, but could be particularly well suited for use with spectroscopy. While spectral contributions can be discriminated, they tend to be collected within a common time window. In cases such as laser-induced breakdown spectroscopy spectral contributions can appear at different times—as a laser induced plasma cools and excited atoms cascade down through energy levels—but this cannot be seen without temporal discrimination, only by iterative repeating with a moving time window. This technique could also be applicable to fluorescence studies where fluorescence lifetimes are relatively long. The micromirror array-based streak camera can in principle capture temporal and spectral data in a single "shot" overcoming the need for repetition and sample damage. Clearly more development is required to improve the achievable resolution and to better understand the diffraction patterns produced, but the principle of using "a projector and a camera" to obtain near nanosecond and nanometer resolution has been established.

Acknowledgments

This work was published by the UK MoD Defence and Security Accelerator.

References

1. L. J. Hornbeck, "Current status of the digital micromirror device (DMD) for projection television applications," in *Proc. IEEE Int. Electron Dev. Meeting*, IEEE, pp. 381–384 (1993).
2. D. Dudley, W. M. Duncan, and J. Slaughter, "Emerging digital micro- mirror device (DMD) applications," *Proc. SPIE* **4985**, 14–25 (2003).
3. D. L. Graff and S. P. Love, "Real-time matched-filter imaging for chemical detection using a DMD-based programmable filter," *Proc. SPIE* **8618**, 86180F (2013).
4. P.-A. Blanche et al., "DMD as a diffractive reconfigurable optical switch for telecommunication," *Proc. SPIE* **8618**, 86180N (2013)
5. J. Ma, "Single-pixel remote sensing," *IEEE Geosci. Remote Sens. Lett.* **6**(2), 199–203 (2009).
6. G. Ritt and B. Eberle, "Automatic laser glare suppression in electro-optical sensors," *Sensors* **15**(1), 792–802 (2015).
7. D. M. Benton, "Multiple beam steering using dynamic zone plates on a micro-mirror array," *Opt. Eng.* **57**(7), 1–13 (2017).
8. M. Mohagheghian and S. G. Sabouri, "Laser wavelength measurement based on a digital micromirror device," *IEEE Photonics Technol. Lett.* **30**(13), 1186–1189 (2018).
9. H. Partanen, J. Turunen, and J. Tervo, "Coherence measurement with digital micromirror device," *Opt. Lett.* **39**(4), 1034–1037 (2014).
10. T. Yoon et al., "Emerging applications of digital micromirror devices in biophotonic fields," *Opt. Laser Technol.* **104**, 17–25 (2018).
11. Z. Zhuang and H. P. Ho, "Application of digital micromirror devices (DMD) in biomedical instruments," *J. Innov. Opt. Health Sci.* **13**(6), 1–22 (2020).
12. V. Lerner et al., "Shaping Laguerre–Gaussian laser modes with binary gratings using a digital micromirror device," *Opt. Lett.* **37**(23), 4826–4828 (2012)
13. M. Mirhosseini et al., "Rapid generation of light beams carrying orbital angular momentum," *Opt. Express* **21**(25), 30196–30203 (2013).
14. E. Anzuola and A. Belmonte, "Generation of atmospheric wavefronts using binary micromirror arrays," *Appl. Opt.* **55**(11), 3039 (2016).
15. D. Benton, "Aberration and coherence effects with a micromirror array," *Proc. SPIE* **11867**, 118670D (2021).
16. Y. X. Ren, R. De Lu, and L. Gong, "Tailoring light with a digital micromirror device," *Ann. Phys.* **527**(7–8), 447–470 (2015).
17. S. Scholes et al., "Structured light with digital micromirror devices: guide to best practice," *Opt. Eng.* **59**(4), 041202 (2019).
18. M.-C. Park et al., "Properties of DMDs for holographic displays," *J. Mod. Opt.* **62**(19), 1600–1607 (2015).
19. B. Hellman and Y. Takashima, "Angular and spatial light modulation by single digital micromirror device for multi-image output and nearly-doubled étendue," *Opt. InfoBase Conf. Pap. Part* **F144**(15), 21477–21496 (2019).
20. B. Hellman et al., "Single-chip holographic beam steering for lidar by a digital micromirror device with angular and spatial hybrid multiplexing," *Opt. Express* **28**(15), 21993 (2020).
21. J. Rodriguez et al., "Fast laser beam steering into multiple diffraction orders with a single digital micromirror device for time-of-flight lidar," *Appl. Opt.* **59**(22), G239 (2020).
22. V. P. Andrianov et al., "Rotating mirror digital streak camera for investigation of fast processes," *Combust. Explosion Shock Waves* **54**(5), 618–623 (2018).
23. M. Allgaier et al., "Streak camera imaging of single photons at telecom wavelength," *Appl. Phys. Lett.* **112**(3), 031110 (2018).
24. D. Qi et al., "Single-shot compressed ultrafast photography: a review," *Adv. Photonics* **2**(01), 014003 (2020).

25. J. E. Harvey and R. N. Pfisterer, "Understanding diffraction grating behavior: including conical diffraction and Rayleigh anomalies from transmission gratings," *Opt. Eng.* **58**(8), 087105 (2019).

David M. Benton graduated in physics from the University of Birmingham in 1989. He completed a PhD in laser spectroscopy for nuclear physics in 1994 and then conducted postdoctoral research in positron emission tomography and then laser spectroscopy for nuclear physics, all at the University of Birmingham. In 1998, he joined DERA, which became QinetiQ, where he worked on a variety of optical projects. He was the leader of a group building quantum cryptography systems and was involved in a notable 140 km demonstration in the Canary Islands. He became chief scientist for L-3 TRL in 2010 working on photonic processing techniques for RF applications. He is now a senior research fellow at Aston University with a variety of interests including free-space optical comms, gas sensing, and laser detection techniques. He is a member of SPIE.